This paper describes objective technical results and analysis. Any subjective views or opinions that might be expressed in the paper do not necessarily represent the views of the U.S. Department of Energy or the United States Government.

SAND2021-7625C

Additive Manufacturing Case Study

Yarom Polsky[1]; Phillip Chesser[1]; Brian Post[1]

Jiann Su[2]

[1]Oak Ridge National Laboratory

[2]Sandia National Laboratories

Keywords: *Geothermal, Additive Manufacturing, Downhole tools*

ABSTRACT

Geothermal technologies include an extremely wide range of products required for well construction, completion, production, intervention and surface energy conversion activities. Many of these products are geometrically complex, require multi-step and highly specialized fabrication processes, and are expensive due to the low production numbers typically associated with the geothermal market. These challenges along with the high temperature demands of the geothermal environment have also hindered the adoption of many tools routinely used in the oil & gas industry.

Recent advancements in Additive Manufacturing (AM) materials of construction, build volumes and part quality have transitioned the technology from primarily cosmetic prototyping applications to the point where AM can be used to make production parts, even for the most demanding applications. These improved AM capabilities along with the inherent ability of AM to produce complex parts and, in some cases, geometries that cannot be manufactured using conventional casting, machining and joining fabrication approaches motivate an exploration of its potential to positively impact geothermal well construction and operations technologies.

Sandia National Labs collaborated with Oak Ridge National Laboratory on a case study examining additive manufacturing opportunities for Geothermal applications. The study focused on designing components with improved performance characteristics that cannot be fabricated conventionally. A rotor for a downhole motor was chosen based on the potential for improving its rotational dynamics. Topology optimization was used as a design method to reduce the rotational inertia of the part while preserving sufficient rotational stiffness to transmit the torque required for the drilling application. The optimization resulted in a nearly 50% reduction in polar moment of inertia while maintaining other desired performance characteristics. The design developed using the topology optimization approach was fabricated using additive manufacturing and cannot be fabricated conventionally. This paper will discuss the design approach, performance improvements and manufacturing methods used to produce the part.

Background/Introduction

Geothermal technologies include an extremely wide range of products required for well construction, completion, production, intervention and surface energy conversion activities. Many of these products are geometrically complex, require multi-step and highly specialized fabrication processes, and are expensive due to the low production numbers typically associated with the

Sandia National Laboratories is a multimission laboratory managed and operated by National Technology & Engineering Solutions of Sandia, LLC, a wholly owned subsidiary of Honeywell International Inc., for the U.S. Department of Energy's National Nuclear Security Administration under contract DE-NA0003525.

geothermal market. These challenges along with the high temperature demands of the geothermal environment have also hindered the adoption of many tools routinely used in the oil & gas industry.

Recent advancements in Additive Manufacturing (AM) materials of construction, build volumes and part quality have transitioned the technology from primarily cosmetic prototyping applications to the point where AM can be used to make production parts, even for the most demanding applications. A number of prior studies have highlighted the potential benefits of AM for the oil and gas industry, an industry that utilizes technology identical or similar to the geothermal industry [Camissa (2014), Sireesha (2014), Vendra (2018)]. These AM benefits include the ability to more economically produce complex parts (in some cases the geometries cannot be manufactured using conventional fabrication methods), the design and fabrication of assemblies with fewer parts, the reduction of material cost and waste associated with manufacturing, and a reduction in costs associated with the logistics of manufacturing complex parts where multiple fabrication processes are utilized.

This attention and benefits described for a related industry motivates an exploration of its potential to positively impact geothermal well construction and operations technologies. Oak Ridge National Laboratory (ORNL) and Sandia National Labs (SNL) recently completed a study of AM application to geothermal technologies [Polsky (2021)]. This study performed a detailed manufacturability and technoeconomic assessment comparing conventional and additive manufacturing of representative geothermal downhole tool parts in order to evaluate the potential benefits of AM for the geothermal industry. In addition to the comparison of conventional and additive manufacturing methods for part production, a design exercise was undertaken by ORNL and SNL to determine if parts taking advantage of AM build complexity could be designed to significantly improve the performance of a geothermal downhole tool.

The ORNL and SNL team performed in-depth design reviews of three SNL downhole tools - two drilling tools and one seismic monitoring tool. The review focused on designing components with improved performance characteristics that cannot be fabricated conventionally. A rotor for a downhole motor was chosen based on the potential for improving its rotational dynamics. Topology optimization was used as a design method to reduce the rotational inertia of the part while preserving sufficient rotational stiffness to transmit the torque required for the drilling application. Topology optimization is a mathematical method for improving the location of material within a structure given a set of design objectives and constraints [Eschenauer (2001)]. The optimization resulted in a nearly 50% reduction in polar moment of inertia while maintaining other desired performance characteristics. The design developed using the topology optimization approach was fabricated using additive manufacturing and cannot be fabricated conventionally. This paper will discuss the design approach, performance improvements and manufacturing methods used to produce the part.

Design Goals

Percussive down the hole hammers (DTHH) are used extensively in the mining, construction, and water well drilling industries and are arguably the best performing drilling technology for hard rock drilling. Percussive devices have among the lowest mechanical specific energies of any drilling method and a reputation for reliable drilling in hard rock. Additionally, torque and weight-on-bit (WOB) requirements are lower than those required in other rock reduction methods. Lower WOB can improve directional stability, and lower torque means less energy input required for

drilling. Both factors have the potential to drive down drilling costs associated with geothermal resource exploration by improving penetration rates and allowing drillers to access difficult to reach geothermal resources.

The auto indexing tool used in the additive manufacturing case study has been designed to operate in the low-torque percussive environment in which DTHH operate. The tool generates impulsive torque to coincide with the percussive action of the hammers. This results in discrete rotational indexing action at the face of the bit. Due to its compact size and form factor, it can also enable advanced techniques, such as directional drilling while taking advantage of the benefits of percussive hammers.

The auto indexer consists of a power generation section, power delivery section and a bearing, and uses a rotational impulse load to generate rotation at the bit. The power section consists of a vane motor, driven by a working fluid (e.g., gas, liquid) (see Figure 1). The vane motor delivers power by transferring angular momentum generated by the fluid through the power delivery section. The power delivery section is composed of hammering elements that strike a shaft to generate rotation in the desired drilling component. The bearing section provides rotational and axial support to the driven shaft.

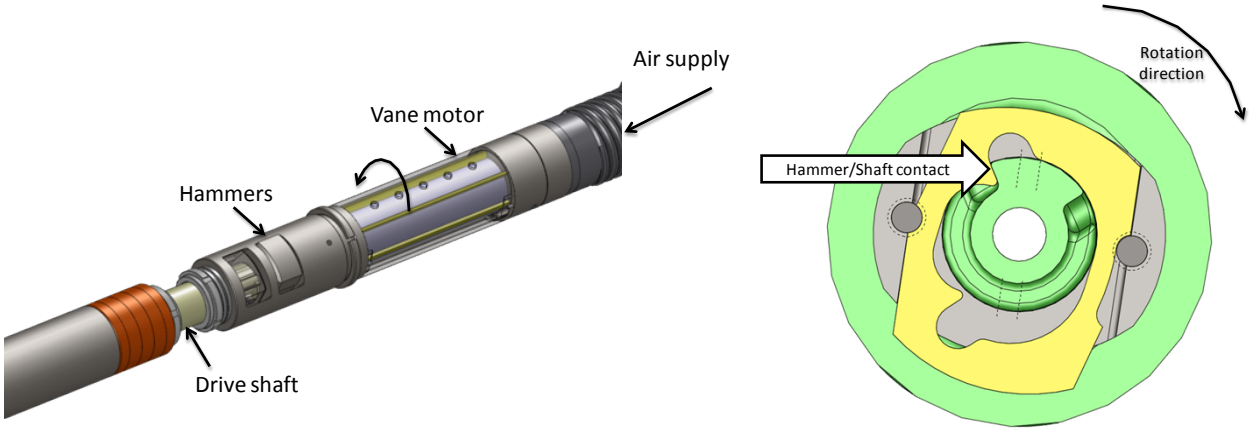

Figure 1. Rotating hammer schematic

One advantage of the impulsive motor is that higher peak torques can be achieved compared to conventional motors for the same supply pressure. Depending on the specific motor geometry, the peak torque produced by a rotational hammer could be up to 60 times higher than a conventional motor [24]. This extra torque would be beneficial in DTHH or for other high peak torque applications.

The inline configuration for the auto indexer requires a flow path through the driving components to power the percussive hammer. Plumbing a conduit for this flow path requires having a hollow rotor for the vane motor as shown in Figure 1. Additional external loading includes the rebound shock loads from the percussive hammer.

Tribological issues—friction, lubrication, and durability—are also important considerations in the overall design of the tool. Traditional lubricants begin to break down under geothermal operating conditions, which is one of the main reasons for temperature limitations in downhole tools. Several of the key design features and limitations are listed in Table 1.

Table 1. Advantages and Disadvantages of Key Design Features of the Auto Indexer

Advantages	Disadvantages
• High-temperature capable • Elastomer-free operation • Standard connections (American Petroleum Industry specifications) • Compact design • High peak torque	• Intermittent rotation • Additional shock loading in the bottom hole assembly (BHA) • May have difficulty in compliant mediums • Does not address other limitations of hammers in geothermal drilling

Early prototypes highlighted several operational considerations required to maximize the output of the motor. Back pressure on the vane motor is extremely detrimental. Allowing free flow of air through the system is crucial to the function of a vane motor. Also, material selection is significant in the overall function of the components because the impacting elements experience repeated impact loads and must have high hardness and toughness values. The impacting surfaces require hardness values on the order of 60 HRC, while the yield strength requirements exceed 100 ksi (~6.9 mPa). These requirements limit potential material choices to heat-treated steels or surface treatment.

With respect to physical properties such as density which affect the dynamic behavior, there is very little if any variation available when considering traditional fabrication techniques.

The component being evaluated for the case study is the rotor at the heart of the vane motor. It serves several functions within the overall indexer including the impulsive force generation. As a result, the physical demands on the part require high hardness and strength. The tolerances are also critical to the overall performance of the motor. Clearances on the order of 12.7 microns (0.0005 in) are required to create the dynamic seals within the stator.

Geometry Optimization

Traditional topology optimization uses an algorithmic optimizer to remove mass in order to optimize around a certain set of objectives, such as maximizing stiffness while minimizing mass. This approach can produce design solutions that are better than human intuition in cases where there is complex geometry or loading. For this design study, the objective is to reduce the mass moment of inertia about the axis of rotation while maximizing the resistance to radial deformation throughout the part. For a rotationally symmetric part, reducing mass moment of inertia reduction simply involves reducing the amount of part mass away from the axis of rotation. A redesign based on human intuition can easily achieve this design objective alone. However, the presence of the vane slots complicates simultaneously optimizing this design objective while minimizing the part's resistance to radial deformation. This is a task better suited to topology optimization.

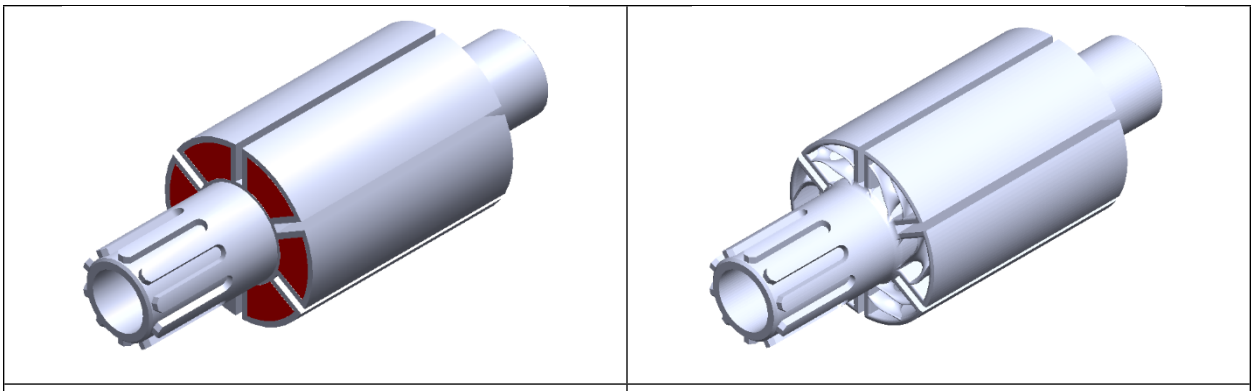

a. Standard solid construction | **b. Topology optimized**

Figure 2. Rotor models (standard vs. topology optimized)

In Figure 2a, area towards the periphery of the part that is not functional is identified for reduction and is shown in red. Full removal of this area would reduce the stiffness of functional surfaces, so this is replaced with a less dense lattice structure instead. This internal area was replaced with a triply minimal periodical surface (TMPS) lattice. A TPMS lattice was used since it has curving surfaces that minimize stress concentrations and sharp corners. The TPMS lattice was generated using nTopology software. The drill rotor design with the internal lattice is shown in Figure 2b. Mass moment of inertia about the primary axis was reduced from 8.5 lb-in^2 to approximately 4.8 lb-in^2 for roughly a 45% reduction.

Calculated Performance Improvements

Analysis of the rotating hammer system begins with the vane motor. A cross-section of the vane motor is shown in **Error! Reference source not found.**. The motor rotates due to pressure differences in the chambers. A rotor is mounted with an eccentricity E_V with respect to the stator. The eccentricity creates variable volumes between neighboring vanes, and the pressure differences result in a non-zero net force, producing rotation. The seal between the vanes and the stator is created by either spring forces or air pressure. The motor can be designed to operate in both single direction and reversible modes.

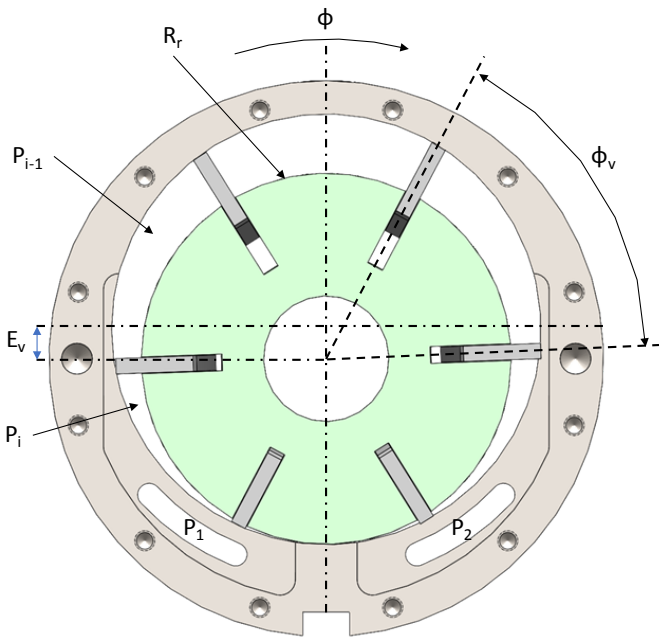

Figure 3. Vane motor cross-section

Given an input pressure P_1 and outlet pressure P_2, the moment delivered by the motor is given by Equation EQ7-1. In the equation, C_M is a geometric parameter, L_V is the length of the motor, and Z_V is the number of vanes:

$$M_M = \frac{\left(C_M \cdot R_R^2 \cdot L_V \cdot Z_V\right)}{(2\pi)}(P_1 - P_2) \qquad \textbf{Eq. 1}$$

The geometric parameter C_M is given by:

$$C_M = \frac{1}{a_m}\left[\begin{array}{c}\varphi_V\left(a_m + \frac{1}{2}\right) - 2\left(a_m + 1\right)\cos\left(\varphi_1 + \frac{\varphi_V}{2}\right)\sin\left(\frac{\varphi_V}{2}\right) \\ + \frac{1}{2}\cos\left(2\varphi_1 + \frac{\varphi_V}{2}\right)\sin\left(\beta_m\right)\end{array}\right] \qquad \textbf{Eq. 2}$$

where $a_m = R_R / H_V$, φ_V is the angle between vanes, and φ_1 is the angle at the end of the charging process.

For a given applied torque, the acceleration of the rotor is inversely proportional to the mass moment of inertia I. It is expected that the lower mass moment of inertia will result in more impacts per minute (IPM). Higher IPM values should result in a higher net output rotational speed. The applied torque is inversely proportional to the mass moment of inertia of the rotor.

$$I\alpha = \tau \qquad \textbf{Eq. 3}$$

Mathematical models for describing the behavior of vane motors are available in the text [Krivts]. Several of the key parameters that determine the overall performance include the size of the rotor

(R_r) and stator (R_s), the length of the vane motor (L), the number of chambers (N), and the rotational inertia of the rotor (I). A first-order relationship between the angular acceleration (α) and applied torque (τ) is given in Eq 3**Error! Reference source not found.**.

A set of differential equations describing the state of the air in each of the chambers must be solved to determine the differential pressure in each of the chambers as the rotor spins. The total torque of the motor is the sum of each of the torques in the adjacent chambers.

A model was developed to solve for the vane motor torque based on the geometry illustrated in **Error! Reference source not found.**. The set of differential equations was solved using a Runge-Kutta integration scheme, with the results of the vane motor rotational speed and torque shown in Figure 2 and Figure 4.

Table 2. Model Parameters used in Simulation

Parameter	**Value (SI Units)**	**Value (Imperial Units)**
I_{std}	.00249 kg-m^2	8.51 lbm-in^2
I_{top_opt}	.00145 kg-m^2	4.8 lbm-in^2
R_r	.0381 m	1.50 in
R_s	.0445 m	1.75 in
L	.102 m	4.0 in
P_1	~10,342 kPa	150 psi
P_2	0 kPa	0 psi

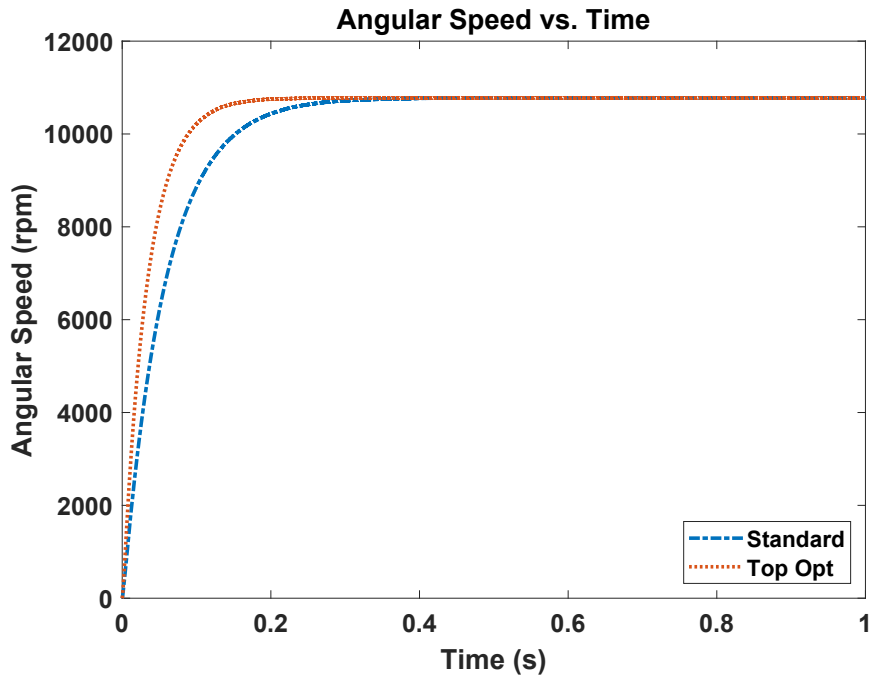

Figure 4. Rotor speed vs. time (standard and topology optimized)

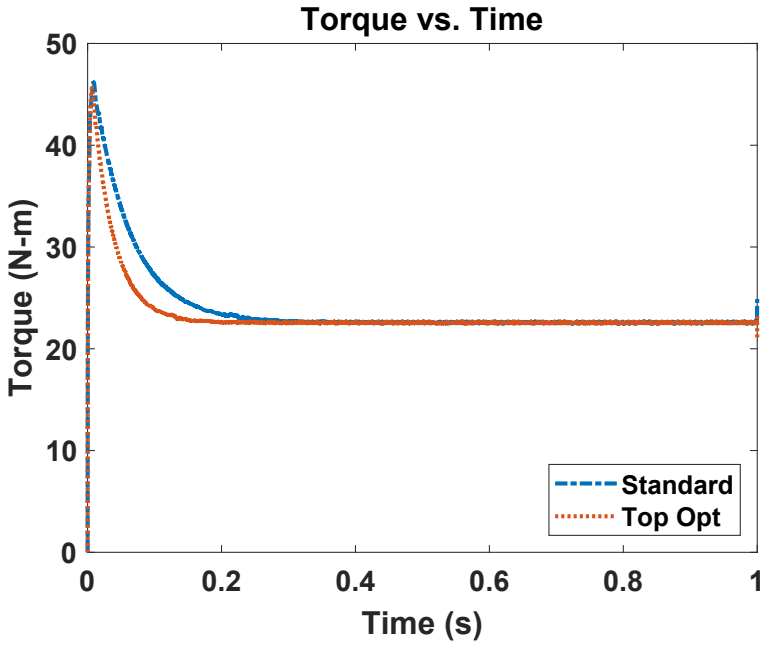

Figure 5. Rotor torque vs. time (standard and topology optimized, 150 psi supply)

As expected, the rotor with the lower rotational inertia reaches steady-state faster than the standard rotor. The difference in acceleration is directly related to the rotational inertia. Additionally, the torque is maximum during acceleration then drops off as the rotor reaches a steady speed.

Manufacturing

The drill rotor was fabricated with Laser Powder Bed Fusion (LBPF) AM using an AddUp FormUp 350 machine. The material used was gas atomized 18Ni300 Maraging steel from Carpenter Additive. This material has a combination of high strength and high hardness that is achievable in the hardened state making it suitable for the application and has good AM printing characteristics.

The dimensional tolerances and surface finish requirements for certain features of this part exceed the capabilities of metal AM systems today. To achieve these requirements, the entire external surface of the part was machined after printing. The external surfaces were overbuilt by 0.050" to provide stock for machining. Also, the threads and spline were filled in with solid material during printing and machined afterwards. LPBF processes cannot accommodate horizontal overhangs in printing, so a chamfer was added to support the large horizontal overhang in the part during printing and post machined to the finished dimensions.

Two drill rotors were printed together standing on end. The print height was 8.15" and took approximately 4 days complete using two lasers. This was longer than would have been necessary due to build pauses. The curved TPMS geometry created a large STL file size that caused memory problems on the FormUp 350's host computer that caused the machine to unnecessarily pause. Upgrading the computer memory on future builds would potentially avoid this. Print time without pausing would be approximately 48 hours. Figure 6 shows the rotors in the FormUp 350 after printing and de-powdering. After machining of one rotor, it was gas nitrided at 440°C for 48 hours to simultaneously nitride the surface and heat treat. Measured hardness on the heat-treated part ranged between 56 HRC to 60 HRC which meets the service requirements.

Figure 6. Parts during additive manufacturing process

The additional stock material that was printed and then removed is illustrated by Figure 7a which shows the as-printed drill rotor and the machined and heat-treated drill rotor side by side. Figure

7b shows the printed TPMS geometry on the interior of the printed and machined rotor. This internal TPMS surface was not machined but left as printed.

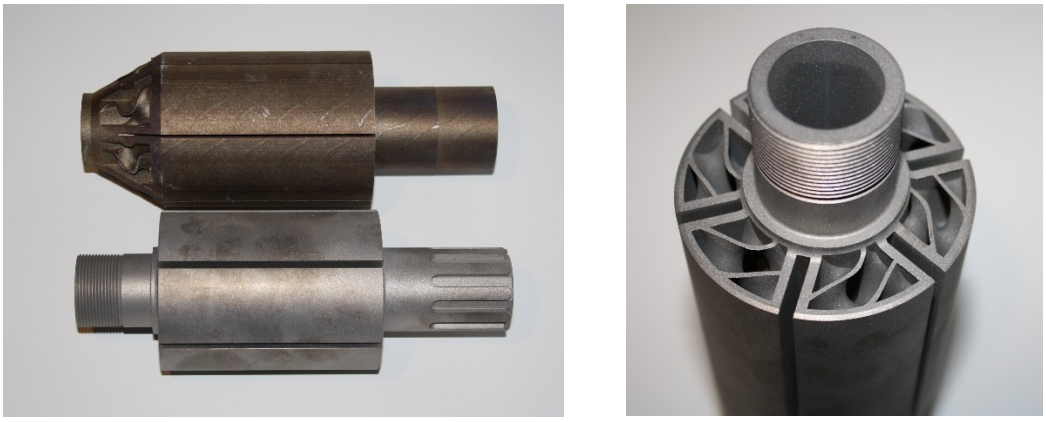

a. As printed **b. Post machining**

Figure 7. Parts as fabricated

Planned Testing

Several controlled tests are planned to characterize the performance difference between the standard machined rotor and the topology-optimized rotor. The first set of tests will be conducted on the Sandia Dynamometer Test Stand (DTS). The test stand consists of a powder brake dynameter and controller Figure 8. A ramp or test sequence is programmed into the controller.

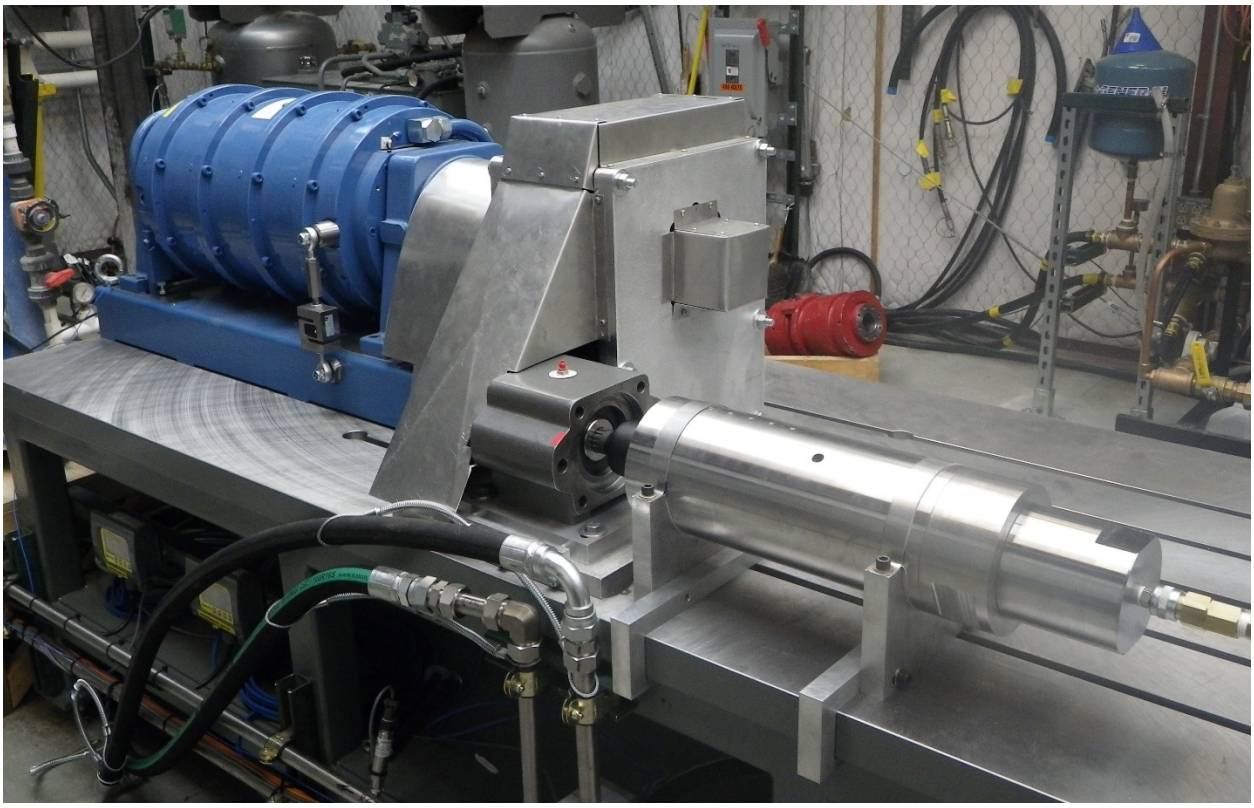

Figure 8. Powder brake dynamometer with vane motor (Magtrol 4PB15).

The dynamometer is powder brake dynamometer that uses magnetic powder in an electric field to produce braking torque. The maximum braking torque is produced at zero speed. The brake dynamometer is rated for 48 kW (64.4 hp).

The vane motor is coupled to the dynamometer through a timing belt and pulley system. The vane motor has an output adapter that attaches to an overhung load adapter. The pulley system produces a 4:1 reduction in input speed compared to the output speed.

Although the maximum torque for each of the systems is expected to be the same, the acceleration of the topology-optimized rotor is expected to be greater proportional to the difference in mass moment of inertia.

In addition to the vane motor test, the effect of the rotor on the overall tool performance will also be assessed. Characterizing and quantifying the torque output of an impulsive motor like the auto indexer presents its own set of challenges. Conventional dynamometers used for measuring motor or torque output are intended to react to constant rotation, which is counter to the discrete movement generated by the auto indexer.

An alternate approach to measuring the torque output is to leverage the relationship between torque applied to a fastener and the resulting axial load. This relationship is commonly used to prescribe bolt torque to reach a desired preload in fastened joints:

$$T = F \cdot K \cdot d \qquad \textbf{Eq. 4}$$

In Eq. 4, K is the torque coefficient, d is the diameter of the fastener, and F is the measured axial force. For this effort, the torque coefficient is assumed to be 0.2 which is typical of metal to metal fasteners.

The test apparatus is shown in Figure 9. It consists of a steel plate bolted to a fixed foundation. In this case, the foundation is a block of granite buried in the soil. The plate is tapped with a thread pattern that matches the driven fastener. A donut-style load cell is captured between the bolt and the plate.

Figure 9. Load cell and bolt torque test fixture

For each test, the bolt is hand tightened to secure the test setup. Then the motor is positioned loosely over the bolt, and the socket is oriented to slide over the bolt. A pressure set point is selected based on the test matrix. The pressure is applied, and the motor can impact for approximately 5–10 seconds. Afterwards, the air pressure is shut off, and the motor is backed away from the bit. The resulting axial force is read from a digital display with force displayed in lbf.

Discussion

Physical properties of the AM prototype were compared to the conventionally manufactured rotor. The measured mass of both parts from the models was within 1.6% of the models. This was compared to the modeled value in Solidworks. The mass moments of inertia were taken from the respective modeling software.

This case study focused on a single component within the overall auto indexer assembly. The reduction in rotational inertia will likely lead to an increase in rotational acceleration when the dynamometer tests are conducted. However, we anticipate that the peak torque increase in the tool will be more modest. Modeling estimates of the impact on peak torque show performance improvements in the single digit percentage. This is because the lighter rotor carries less momentum than the solid part. The net result is a modest increase in the transfer of angular momentum between the standard and AM parts.

This leads to a salient point when considering AM during the design process. Realizing the true benefits of AM requires consideration of design and manufacturing for the entire product assembly. While this typically applies to design goals of reducing overall part count and assembly complexity, it can also apply to design goals associated with performance improvement. The benefits gained from using AM for individual components provides a less compelling case for the use of the production technique.

Summary and Conclusions

An additive manufacturing case study was conducted on a downhole rotation tool. The case study assessed the potential benefits of using additive manufacturing. A rotor from a downhole motor was evaluated, designed, and fabricated using AM techniques. A standard part was compared with an AM part with the same overall geometry. Tests were planned to characterize the performance gains resulting from the AM process. Design targets for the AM part were intended to match those of the conventional part. These targets included surface hardness, yield strength, and dimensional tolerances and surface finish. A reduction in rotational inertia was achieved through topology optimization and power bed fusion AM fabrication.

At the time of the paper submission, the tests had not been conducted. Additional fixturing and hardware are needed to interface with the test hardware. They are currently in production, and the tests are expected to be conducted in Q3-Q4 of FY 2021.

References

Beccu, R.S. 2003. Percussive Rotational Impact Hammer. Patent # 6,609,577 B2.

Camissa, J.A., Verma, V., Marler, D.O. and Madlinger, A. (2014). Additive Manufacturing and 3D Printing for Oil & Gas – Transformative Potential and Technology Constraints. *Twenty-fourth International Ocean and Polar Engineering Conference*, Busan, Korea.

Eschenauer H.A. and Olhoff, N. (2001). Topology Optimization of Continuum Structures: A Review. *Appl. Mech. Rev.,* Vol. 54, No. 4, pp. 331- 390.

Krivts, I.L., & Krejnin, G.V. (2006). Pneumatic Actuating Systems for Automatic Equipment: Structure and Design (1st ed.). CRC Press. https://doi.org/10.1201/9781420004465

Polsky, Y., Armstrong, K., Price, C., Su, J., Wang, A., Post, B., and Chesser, P. (2021). Study of Additive Manufacturing Applications to Geothermal Technologies Final Project Report. https://doi.org/10.2172/1778076

Sireesha, M., Lee, J., Kiran, A., Babu, V.J., Kee, B.T. and Ramakrishna, S. (2018). A Review of Additive Manufacturing and its Way into the Oil and Gas Industry. *RSC Advances*, Issue 40.

Vendra,L. and Achanta, A. (2018). Metal Additive Manufacturing in the Oil and Gas Industry.

Funding Statement

This paper describes objective technical results and analysis. Any subjective views or opinions that might be expressed in the paper do not necessarily represent the views of the U.S. Department of Energy or the United States Government.

Sandia National Laboratories is a multimission laboratory managed and operated by National Technology & Engineering Solutions of Sandia, LLC, a wholly owned subsidiary of Honeywell International Inc., for the U.S. Department of Energy's National Nuclear Security Administration under contract DE-NA0003525.

Research supported by the Geothermal Technologies Office, Office of Energy Efficiency and Renewable Energy, U.S. Department of Energy under contract DE-AC05-00OR22725, Oak Ridge National Laboratory, managed and operated by UT-Battelle, LLC.